Journal of Aeronautics & Aerospace Engineering
ISSN: 2168-9792

Alsarheed and Sedaghat, J Aeronaut Aerospace Eng 2016, 5:1
DOI: 10.4172/2168-9792.1000161

Research Article Open Access

Computational Study of Ailerons in Cross Flows Ground Effects and Biplanes Configurations

Alsarheed M* and Sedaghat A

Department of Mechanical Engineering, Australian College of Kuwait Mishref, Kuwait

Abstract

An aileron, part of the trailing edge of a fixed-wing airplane, is used to control aircraft's movement around its longitudinal axis (roll). Ailerons have significant impacts on airfoil surface pressure and its lift and drag coefficients. Both panel and finite volume methods were used on a NACA 2412 airfoil with a 20% aileron in a cross flow. The aerodynamic performance of ailerons alone, in a biplane configuration, and in the ground effects has been computationally investigated using both the panel and the finite volume methods. Several parameters were analyzed including the effects of the attack angle of the airfoil, aileron deflection angle, the ride height from the ground, and the characteristics of biplanes. Results of both computational methods are presented and discussed for the aforementioned configurations of NACA 2412 airfoil with aileron.

Keywords: Aileron; Biplane; Finite volume; Ground effect; NACA 2412; Panel method

Introduction

From flying a kite to operating a hypersonic vehicle, achieving and maintaining a high lift is always critical to a successful performance of a flying craft. Some of the advantages of an efficient lift system include improved maneuverability, higher wing payload capacity, longer range for given gross weight, and lower takeoff and landing speeds. Wing components such as trailing edge flaps play a major role in altering lift in conventional fixed-wing aircrafts. They control lift and extend speed range by upward or downward movements causing an increase or decrease in lift. Also, the flap deflection can reduce efficiency by causing or increasing drag, which sometimes is difficult to reduce due to flow with high Reynolds number. Part of the trailing edge assembly is a flap called ailerons, which is a French word for 'little wing' that is used to control the aircraft in its longitudinal axis (roll). This movement is called 'rolling' or 'banking' and it alters the flight path due to the titling of the lift vector. One of the main components that impacts lift is the airfoil. An airfoil is a cross sectional part designed to generate lift when it is subject to an air flow. Ailerons are not just limited to aircraft applications. They are also used in high speed levitation trains to control and maintain the hovering in track.

The airfoil configuration has been widely studied. There are several studies that optimize the airfoil configuration and assess the maximum airfoil lift capabilities [1,2]. Other literatures study the efficiency of the airfoil and the effects of different parameters on it [3]. The camber and the Reynolds number effects have also been studied by many including Levy [4]. Other work done by Birch [5] and Rinoie [6] include calculations of unsteady loading on the airfoil and the effect of trailing edge flaps on flow vortex shapes. Also, the performance of a wing in ground effect and the flow field characteristics has been studied in [7,8]. In addition, the lift distribution between biplane wings and other biplane characteristics have been looked at in [9]. The objective of this paper is to investigate the performance and the ground effects on the ailerons of a biplane configuration. Both panel and finite volume methods were used on a NACA 2412 airfoil with a 20% aileron in a cross flow. Numerical measurements of surface pressure distributions were also obtained to determine the lift and drag coefficients for various configurations.

Airfoils Characteristics

For every action, there is an equal and opposite reaction. According to Newton's third law [10,11] an airfoil generates lift by diverting the motion of flow over its surface in a downward direction, resulting in an equal upward reaction. Typical airfoil geometry is shown in Figure 1.

The main parameters of an airfoil, which play a key role in its aerodynamic performance, are the angle of attack, the chord length, and the mean camber line. The chord is the straight line across the airfoil and it is used to measure the airfoil length. The mean camber is the line halved the airfoil thickness and it is used to measure airfoil curvature.

Common airfoil shapes have been characterized by the National Advisory Committee for Aeronautics (NACA) [12]. Each airfoil shape is defined by this system by a series of digits that correspond to non-dimensional airfoil properties. The number of digits series varies, but in this paper the focus is on four digit airfoils (NACA 2412).

A NACA 2412 airfoil has a maximum camber that is 2% of the chord length with a maximum thickness of 12% of the chord length, located 4/10 of the chord length away from the leading edge.

Computational Modeling

A NACA 2412 airfoil configuration with a 20% aileron was used for the panel and finite volume methods, and it is shown in Figure 2a. The chord length of the airfoil is designated by c, the velocity of the uniform flow is denoted by U, δ_f is the aileron deflection angle, and α represents the angle of attack. The flow is assumed to be two-dimensional steady and incompressible Laminar flow.

***Corresponding author:** Alsarheed M, Department of Mechanical Engineering, Australian College of Kuwait Mishref, Kuwait, Tel: 965 1828225; E-mail: m.alsarheed@ack.edu.kw

Received February 02, 2016; **Accepted** February 26, 2016; **Published** February 29, 2016

Citation: Alsarheed M, Sedaghat A (2016) Computational Study of Ailerons in Cross Flows Ground Effects and Biplanes Configurations. J Aeronaut Aerospace Eng 5: 161. doi:10.4172/2168-9792.1000161

Panel method

The airfoil was analyzed using a vortex panel method, where the airfoil was approximated by a finite number of panels. As shown in Figure 2b, the airfoil surface is divided into 70 panels. There are more panels near the leading and trailing edge to accommodate for the rapid changes in flow near these two ends. Each panel had local, uniform and distributed vortices. Since the velocities can be singular at the center of the vortex, and to avoid singularities, these vortices had infinitesimal strength $\gamma_0 ds_0$, where γ_0 is the vortex strength per unit length, and ds_0 represents the length of a small segment of the airfoil.

The governing equation for the stream function due to all such infinitesimal vortices at a point in space may be given by:

$$\psi = \oint \frac{\gamma_0}{2\pi} \ln\left(\bar{r} - \bar{r}_0\right) \, ds_0 \tag{1}$$

where $\bar{r}_0$ is a point in the x-y plane with coordinates x_0 and y_0 and the distance between the position of the vortex, and the point where the velocity is evaluated with coordinates x and y is denoted by $_{x-y}$. The x-y plane is originated at the leading edge of airfoil with x-axis along chord length and y perpendicular to it.

Equation (1) is integrated over all vortices on the airfoil surface and the stream function associated with the free stream is given by $u_\infty y - v_\infty x$, where u_∞ and v_∞ are the x- and y- components of the free stream velocity. Taken these effects into account, the stream function at any point $\bar{r}$ in space is given by

$$\psi = u_\infty y - v_\infty x - \frac{1}{2\pi} \oint \gamma_0 \ln\left(\left|\bar{r} - \bar{r}_0\right|\right) \, ds_o \tag{2}$$

Since the body itself is a streamline, the stream function value at all the points on the airfoil will be constant and the value is denoted by C. Also, for all points $\bar{r}$ on the airfoil surface, equation (2) becomes:

$$u_\infty y - v_\infty x - \frac{1}{2\pi} \oint \gamma_0 \ln\left(\left|\bar{r} - \bar{r}_0\right|\right) \, ds_0 - C = 0 \tag{3}$$

The Kutta condition is an aerodynamics principle and it is applicable to the trailing edges of the airfoils. This condition states that both the pressure above and below the trailing edge of the airfoil must be equal. It also requires that the flow be smooth and must leave the trailing edge in the same direction at both upper and lower edges and it is expressed as follows:

$$\gamma_{upper} = -\gamma_{lower} \tag{4}$$

For a finite number of N panels, there are equal N unknown vorticity strengths, denoted by $\gamma_{o,j}$, as shown in Figure 2(b). To approximate the line integral over the entire airfoil, it can be integrated as several line integrals over N panels, taking each value of γ_o as constant and so equation (3) becomes:

$$u_\infty y_i - v_\infty x_i - \sum_{j=1}^{N} A_{i,j} \gamma_{0j} - C = 0 \tag{5}$$

$$A_{i,j} = \frac{1}{2\pi} \int \ln\left(\left|\bar{r}_i - \bar{r}_0\right|\right) ds_0$$

Equation (5) can also be solved over the entire airfoil as several line integrals over the panels for the unknown vorticity strengths.

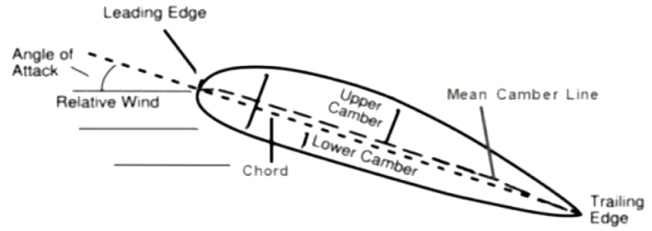

Figure 1: Diagram of an airfoil [11].

Finite volume method

The numerical simulations were conducted using FEMLAB software with a Reynolds number Re = 3×10^6. The Reynolds number Re is defined as

$$\mathrm{Re} = Uc/\upsilon \tag{6}$$

Where U is the velocity of a uniform flow, c is the chord length of the airfoil, and υ denotes the kinematic viscosity

The governing non-dimensional equations for the fluid flow are described by the following continuity and Navier-Stokes equations:

$$\nabla . u = 0$$
$$\rho \frac{\partial u}{\partial t} - \nabla . \upsilon \left(\nabla u + (\nabla u)^T\right) + \rho (u . \nabla) u + \nabla p = 0 \tag{7}$$

Where ρ is the density, u represents the velocity vector, and p is the pressure.

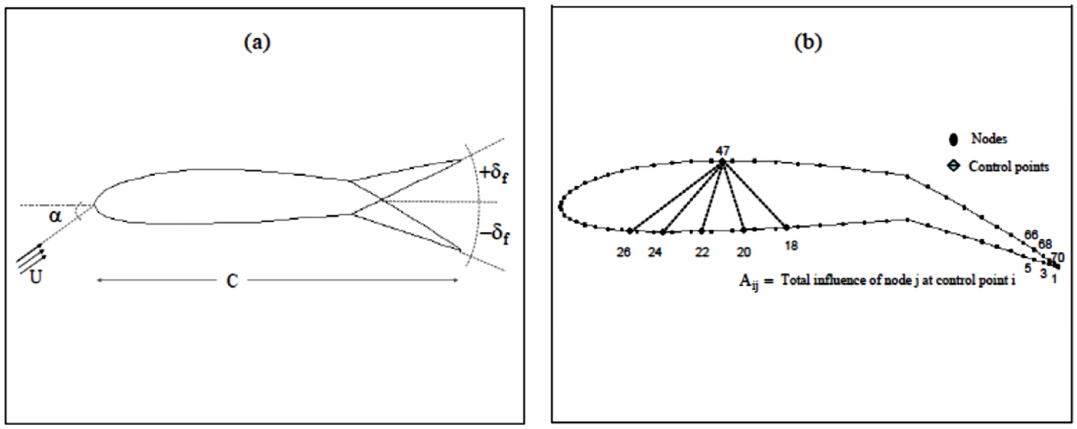

Figure 2a: NACA 2412 Airfoil with aileron, **(b)** Panels for NACA 2412 airfoil with 20% aileron divided into 70 panels.

Results and Discussions

Panel method

Aileron effects: For the zero aileron deflection case ($\delta = 0$), the experimental results of NACA 2412 airfoil with data from Panel code and FEMLAB are compared in Figure 3. The results show a good agreement in all cases and validate the accuracy of the panel method.

Effects of a 20% aileron applied to the NACA 2412 airfoil on the value of lift force and moment coefficients are shown in Figure 4. Figure 4a shows the use of ailerons can change the lift over 50%. Also, by increasing the deflection angle, the drag coefficient increases rapidly. The moment coefficients for different aileron deflection angles are shown in Figure 4b and are based on 25% airfoil chord length. For a constant aileron deflection angle, the moment coefficient stays approximately constant for different attack angles.

Figure 5 shows variation of pressure coefficients for different deflection angles and an incidence angle of $\alpha = 3°$. When the aileron is upward, the pressure coefficient has a considerable change approximately at the middle of the airfoil. For $\delta_f \neq 0$ around 0.8 airfoil length, there are two pressure peaks at the lower and upper surfaces of the airfoil. As it is shown in the figure, the deviation of these pressure peaks from the initial case ($\delta = 0$) is larger when the aileron is downward.

Ailerons in ground effects: Fundamental geometric parameters such as ground clearance, wing camber and its thickness ratio can have impact on the performance of a wing in presence of a solid wall (ground). In Panel method, a wing in ground effect is equivalent to a two-wing case, where the second wing is the mirror image of the first, as shown in Figure 6a, and the wing-body combinations are solved simultaneously. The effect of ride height on the lift coefficient is

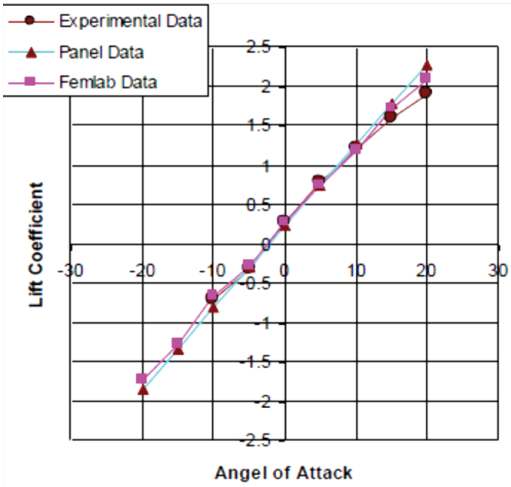

Figure 3: Comparison of lift coefficient between Panel, FEMLAB and experimental data for a NACA 2412 airfoil.

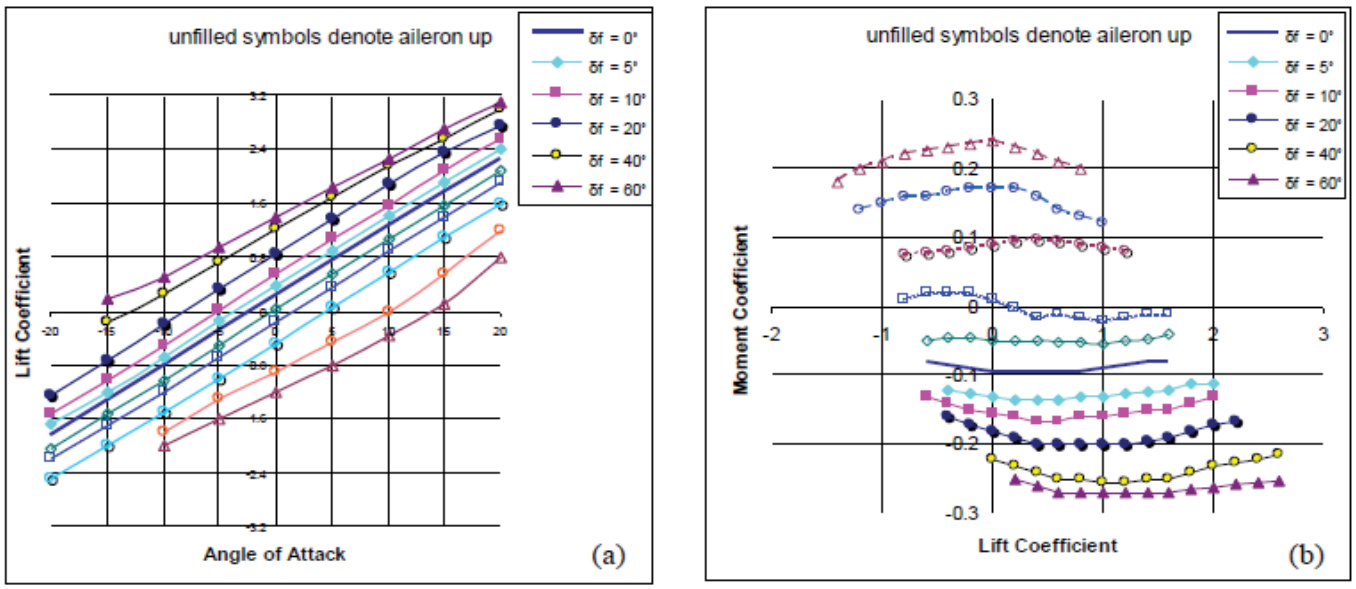

Figure 4: (a) Force Coefficients for a NACA 2412 airfoil with aileron in cross flow (Panel Method), **(b)** Moment Coefficients for a NACA 2412 airfoil with aileron in cross flow (Panel Method).

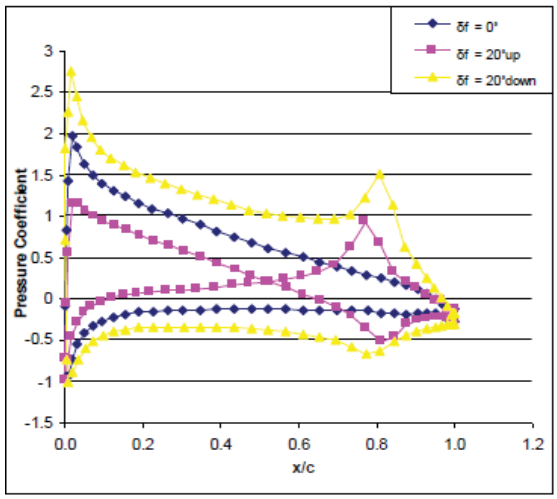

Figure 5: Surface pressure distributions for δ = 0, +20, −20 f and α = 3° (Panel method).

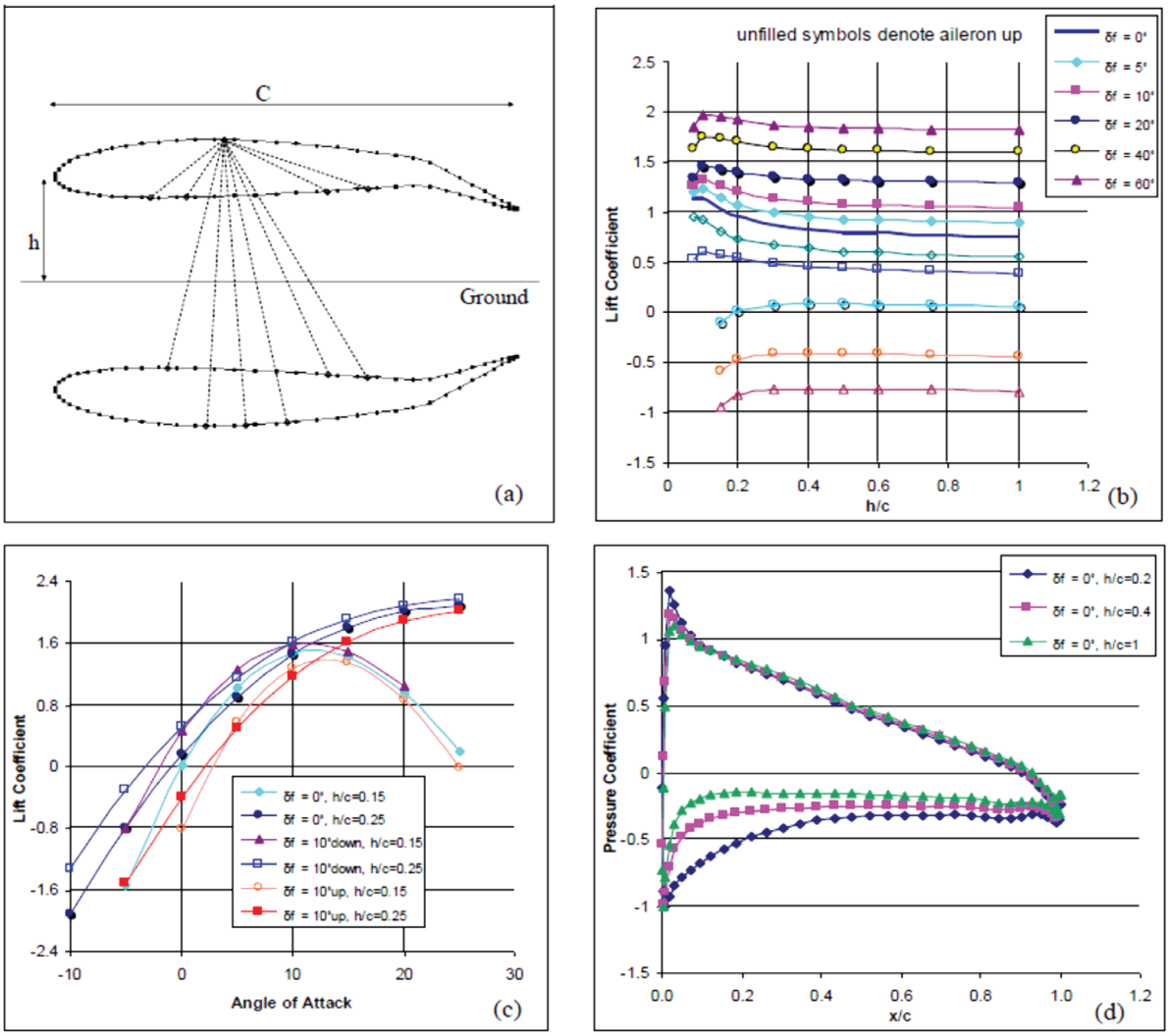

Figure 6: (a) Ground effect (Panel method) **(b)** Lift coefficients in ground effect for different ride heights (Panel method). **(c)** Lift coefficients in ground effect for different configurations (Panel method), **(d)** Pressure coefficients for a NACA 2412 airfoil without aileron (Panel method).

presented in Figure 6b. The tests were performed at an angle of attack of 3°. At a close proximity of the wing to the ground, the effect of higher down force coefficients is clearly noticeable.

The physical effect of the ground is to constrain the airflow on the suction (lower) surface of the wing. This causes an acceleration of the flow compared with the case away from ground effects which results in a greater suction on the lower surface of wing and hence cause a higher lift force. As the ride height decreases, the ground effect causes the flow to be accelerated to a higher degree, generating a significantly higher lift force compared with free stream. At ride heights of less than 0.1*c*, there is a gradual and then significant deviation from the earlier trend of ever-increasing lift force with reduction in ride height. Eventually, the lift force falls off to reach a maximum C_L of 2 at a ride height of 0.1*c*, as shown in Figure 6(b). The effect of attack angle on C_L in ground effect is shown in Figure 6c**.** As it is shown, when the ride height is less than 0.15*c*, the lift coefficient decreases rapidly for α >10° as also observed in ref. [13]. In Figure 6d, C_p distribution of a NACA 2412 without aileron is shown in ground effect. As it is expected, the pressure coefficient in this case only changes at the lower surface of the airfoil for different ride heights.

Figures 7a and 7b show the pressure coefficient (C_p) distribution when the aileron deflection of ± 20° is occurred in the airfoil. For δ_f = -20°, the pressure coefficient of the lower surface changes gradually due to the distance between airfoil and ground. It also decreases when the airfoil is closer to the ground. However, as it is shown in Figure 7b, when δ_f = +20° the pressure coefficient of the lower surface changes rapidly and reaches 8 at the connection of the aileron.

Ailerons in biplanes: The effect of ailerons in biplane configurations on lift coefficient (C_L) is examined using panel method. For a biplane configuration, the surfaces of two airfoils are divided into several N panels. The number of equations is equal to N+2 since there are N panels and (corresponding vortex strength) and two values of stream function C_1 and C_2 for the two airfoils. Also, there are two Kutta conditions, one for each airfoil. Then, the system of equations is set from influence of vortices on each panel and solved. Figure 8a shows the configuration of a biplane with aileron deflection, where the upper and lower airfoils are labeled as 1 and 2 respectively. The difference between aileron deflection in upper and lower airfoils and their effect on the lift coefficient are shown in Figure 8b and 8c. For a high aileron deflection and attack angle, the lift coefficient (C_L) can reach as high as 4. According to the data shown in Figure 8(c), the choice of the airfoil for aileron deflection does not have significant effect on the lift coefficient for h/c >0.5. The pressure coefficient and the difference between aileron deflection of the upper and lower airfoils for α = 3°, δ_f = -20° and h/c = 0.5 is presented in Figure 8d. The results show that when the deflection is on the lower airfoil, the pressure coefficient of the upper airfoil has an unexpected distribution among the surfaces of the airfoil.

Finite-volume method

Aileron effects: The results of NACA 2412 airfoil with data from FEMLAB, for the case where the aileron deflection is equal to zero, are shown in Figure 9. The experimental results and the results from the data generated from FEMLAB for NACA 2412 airfoil are in agreement.

Figure 10 shows the effects of a 20% aileron applied to the NACA 2412 airfoil on the value of lift and moment coefficients. From Figure 10a, it can be seen that the use of ailerons can change the lift over 50% but by increasing the deflection angle, the drag coefficient increase rapidly which is not desired. The moment coefficients for different aileron deflection angles are shown in Figure 10b and are based on a 25% chord length of the airfoil. As it is shown, for a constant aileron deflection angle, the moment coefficient stays approximately constant for different attack angles [14].

Figure 11a and Figure 11b show the values of drag coefficient for different aileron deflection angles. The maximum drag can reach up to 0.24 for δf = - 60° when the lift coefficient is around 2.5, and it occurs when the aileron is downward.

The difference of pressure coefficients for different deflection angles with α = 3° is shown in Figure 12. When the aileron is upward, the pressure coefficient has a considerable change approximately at the middle of the airfoil. Also, there are two pressure peaks at the lower and upper surfaces of the airfoil for $\delta_f \neq 0$. The deviation of these pressure peaks from the normal case ($\delta_f = 0$) is larger when the aileron is downward.

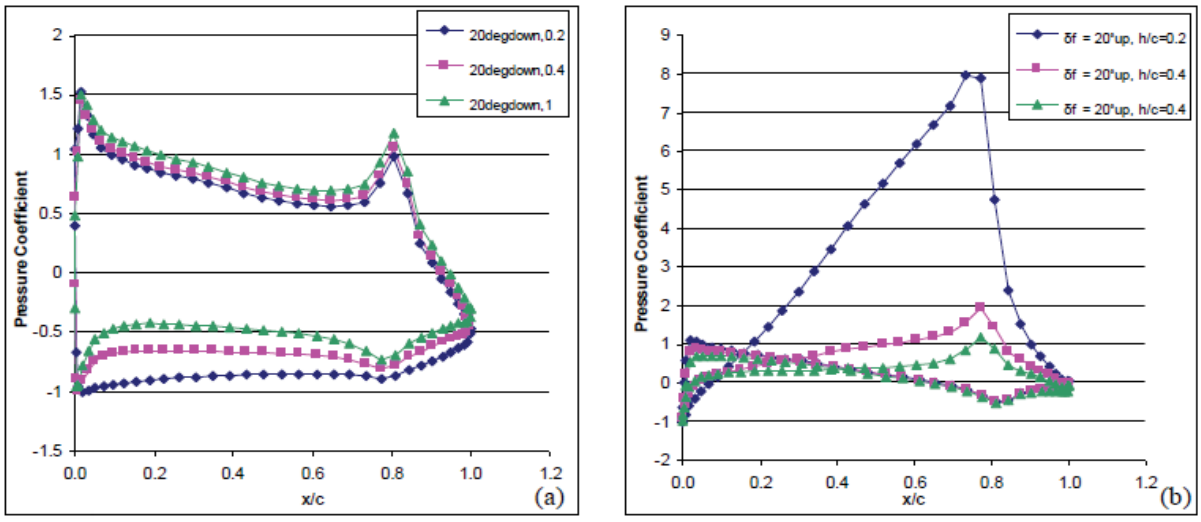

Figure 7: (a) Pressure coefficient distribution for a NACA 2412 airfoil with aileron in ground effect, α = 3° and δf = -20°, (Panel method) **(b)** Pressure coefficient distribution for a NACA 2412 airfoil with aileron in ground effect, α = 3° and δf = +20°, (Panel method).

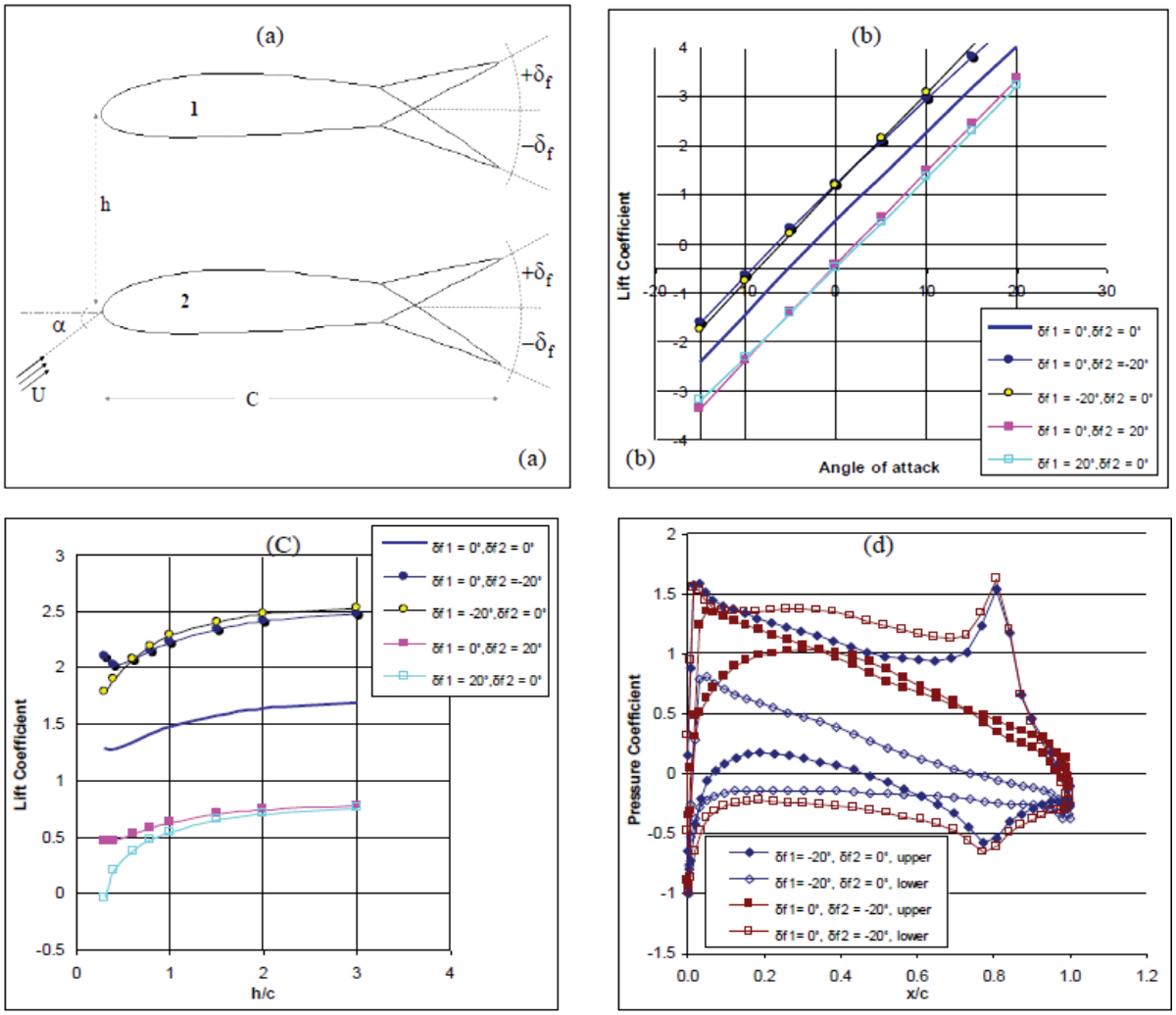

Figure 8: (a) Biplane configuration of NACA 2412 Airfoil with aileron (Panel method) **(b)** Lift coefficients in biplane with aileron deflection due to angle of attack (Panel method). **(c)** Lift coefficients in biplane with aileron deflection due to distance between the airfoils (Panel method) **(d)** Pressure coefficients in biplanes with aileron deflection in different configurations (Panel method).

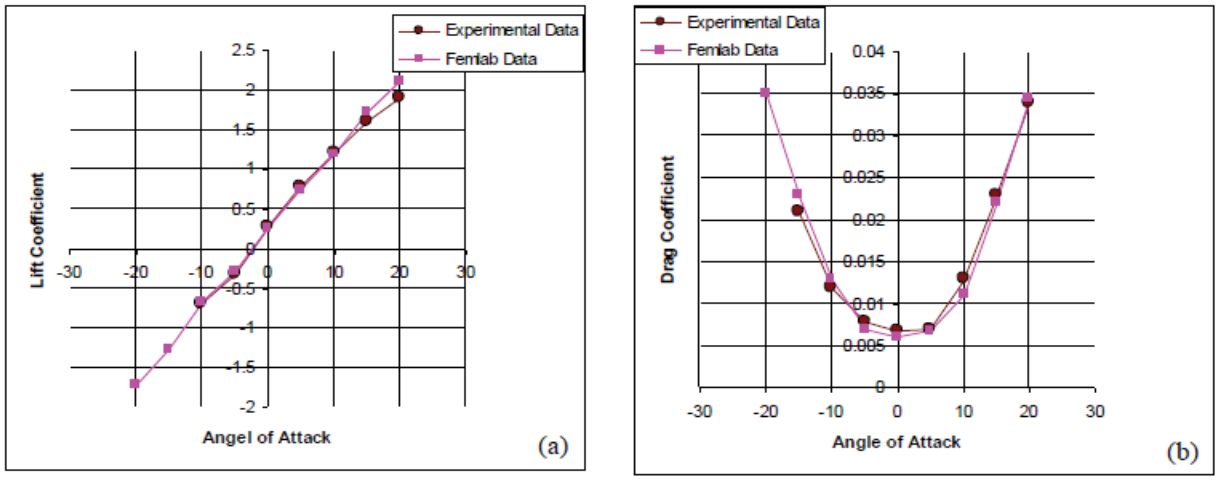

Figure 9: (a) Lift coefficients-experimental and numerical data for a NACA 2412 airfoil **(b)** Drag coefficients-experimental and numerical data for a NACA 2412 airfoil.

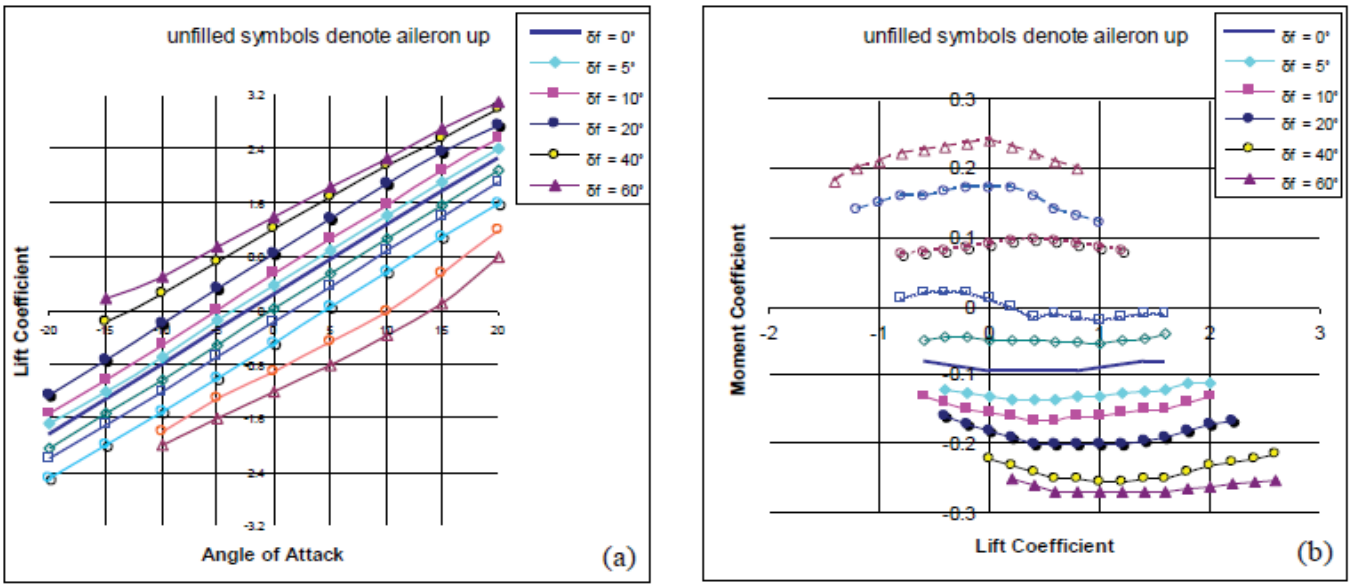

Figure 10: (a) Lift coefficients for a NACA 2412 airfoil with aileron in cross flow (FEMLAB) **(b)** Moment coefficients for a NACA 2412 airfoil with aileron in cross flow (FEMLAB).

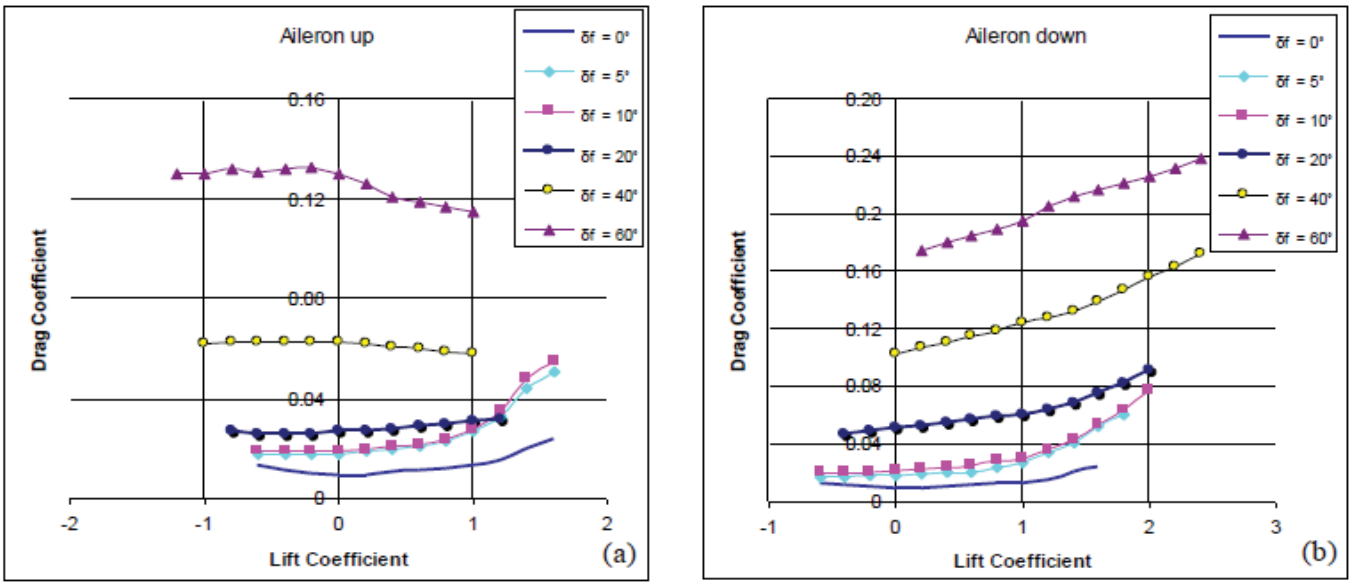

Figure 11: (a) Drag coefficients for a NACA 2412 airfoil with aileron up in cross flow (FEMLAB) **(b)** Drag coefficients for a NACA 2412 airfoil with aileron down in cross flow (FEMLAB).

The flow separation caused by different aileron deflections has also been analyzed. The outflow boundary condition is used at the downstream and the velocity at upstream boundary is selected to be the uniform velocity U. Figure 13a illustrates the airfoil-aileron configuration and the geometry surface grids. Figure 13b shows the effect of aileron deflections on the flow field at three aileron deflections, δ_f = -20, 0 and 20. When the aileron deflection is downward ($\delta_f < 0$), the flow separation occurs earlier with more flow in the upward direction. Then, the flow reconnects again near the trailing edge when the attack angle is very small and forms a small separation region. When the aileron deflection is upward ($\delta_f > 0$), the flow separation happens later with less flow occurs in the upward direction.

Ailerons in ground effect: Wing performance in presence of a solid wall (ground) is affected by some fundamental geometric parameters such as the ground clearance, the wing camber and its thickness ratio. Figure 14 shows flow field velocity contours of ailerons in ground effect.

When the wing is in close proximity to the ground, the effect of higher lift force coefficients is noticeable. Figure 15a shows the effect of ride height on the lift coefficient at an incidence of 3°. The physical

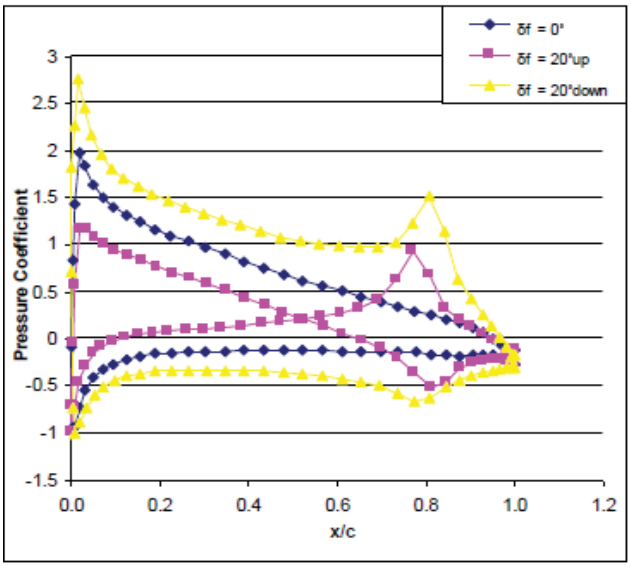

Figure 12: Surface pressure distributions for δf = 0°, +20°, -20° and α = 3° (FEMLAB).

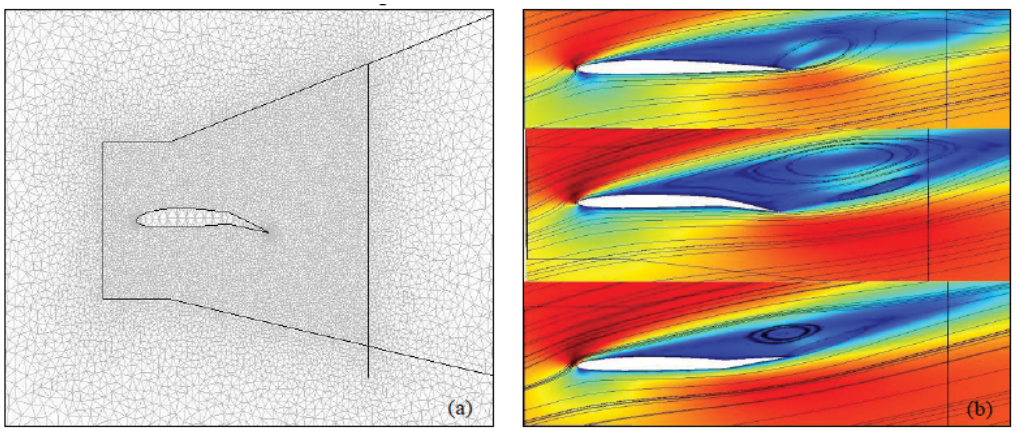

Figure 13: (a) Surface geometry and grids of a NACA2412 airfoil with 20% aileron, δf = -20° **(b)** Flow field velocity contours show separation patterns for different aileron deflections δf = 0, -20, 20, α = 20°.

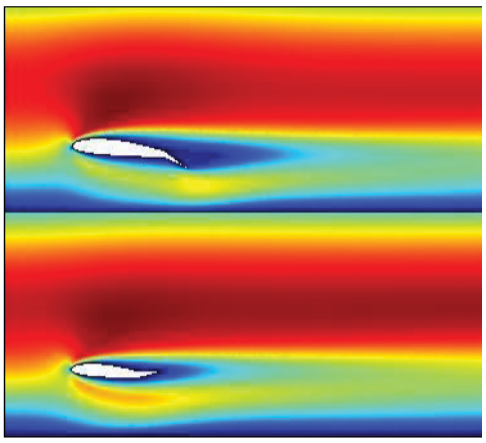

Figure 14: Flow field velocity contours for NACA 2412 airfoil-aileron configuration in ground effect δf = ± 20°, α = 5°.

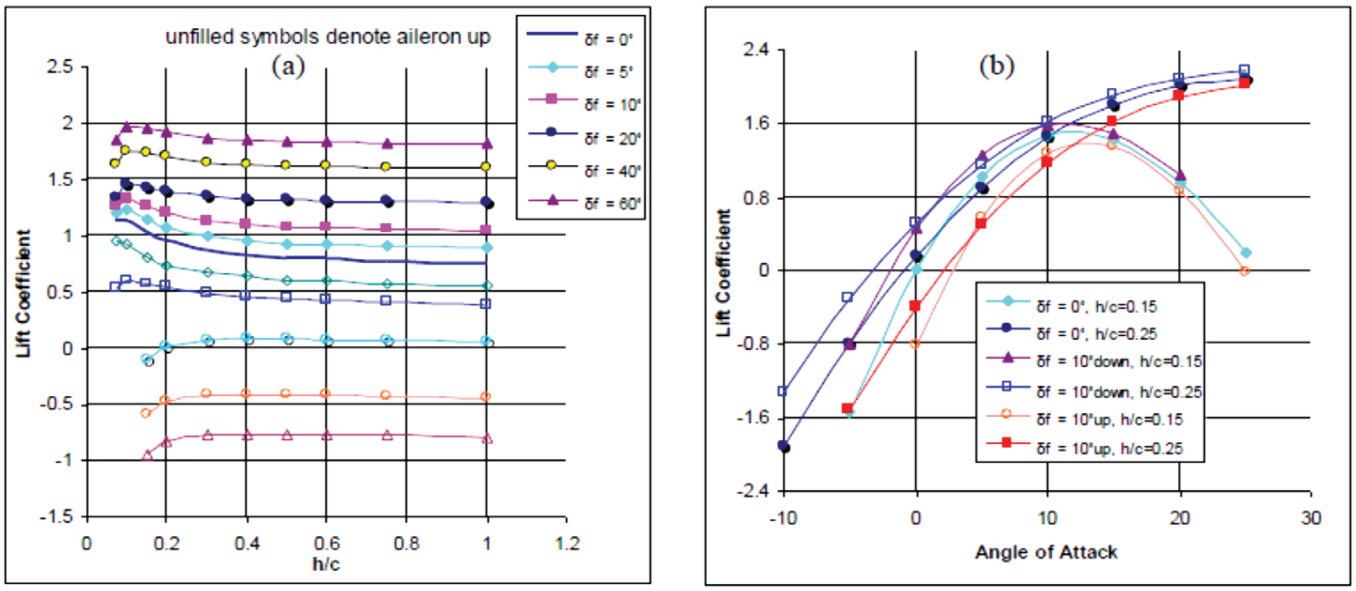

Figure 15: (a) Lift coefficients in ground effect for different ride heights (FEMLAB) **(b)** Lift coefficients in ground effect for different angles of attack (FEMLAB).

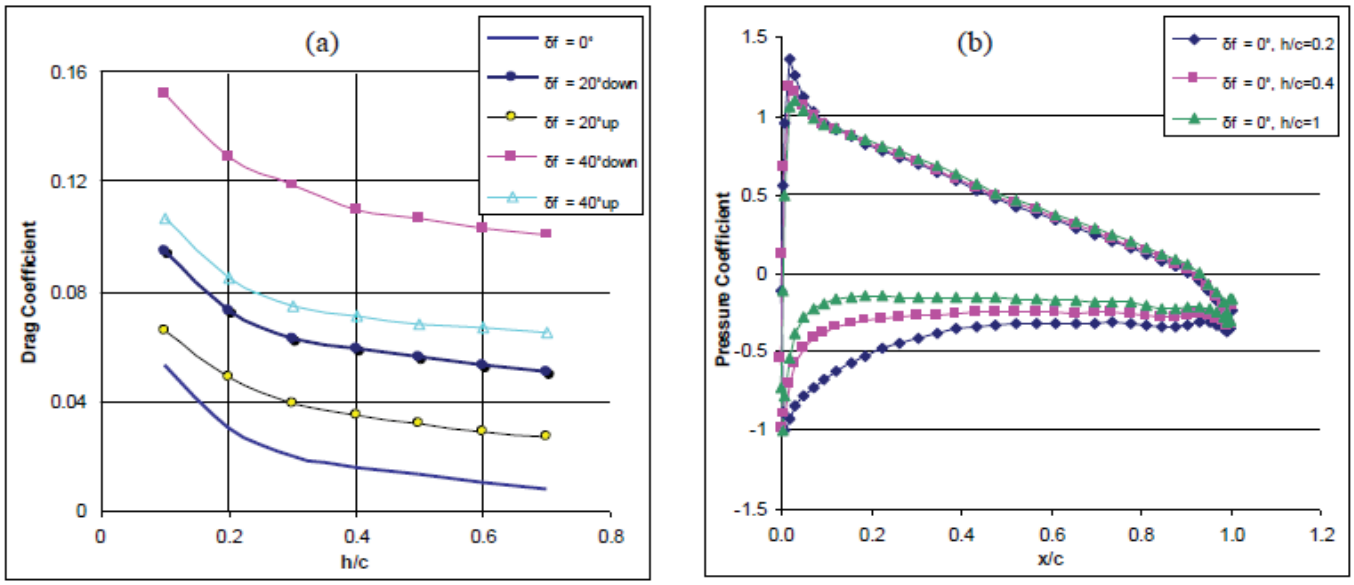

Figure 16: (a) Drag coefficients in ground effect for different ride heights (FEMLAB) **(b)** Pressure coefficients for a NACA 2412 airfoil without aileron (FEMLAB).

effect of the ground is to constrain the airflow over the suction surface of the wing. This causes an acceleration of the flow compared with the case out of ground effect and results in a greater suction on the suction surface and, hence, a higher lift force. As the ride height is reduced, the ground effect causes the flow to be accelerated to a higher degree, generating a significantly higher lift force compared with free stream. At ride heights of less than 0.1*c*, there is a gradual and then significant deviation from the earlier trend of ever-increasing lift force with reduction in ride height. Indeed, the lift force falls off, to reach a maximum C_L of 2, at a ride height of 0.1*c*. The closer it is to the ground, the more lift force reduction is seen. The effect of attack angle on the lift coefficient (C_L) in ground effect is shown in Figure 15b. When the ride height is less than 0.15*c*, the lift coefficient decreases rapidly for $\alpha > 10°$.

The effect of ride height on drag coefficient is shown in Figure 16a at an angle of attack fixed to 3°. As it is expected, when the airfoil is close to the ground, the drag coefficient is high and can reach up to 0.16 for a ride height of 0.1 and $\delta_f = -40°$. In Figure 16b, pressure coefficient (C_p) distribution of a NACA 2412 without aileron is shown in ground effect.

Figure 17a and 17b show the pressure coefficient (C_p) distribution when the aileron takes deflection angle of ± 20°. For $\delta_f = -20°$ case, the pressure of the lower surface changes gradually due to the distance between airfoil and ground and decreases when the airfoil is closer to

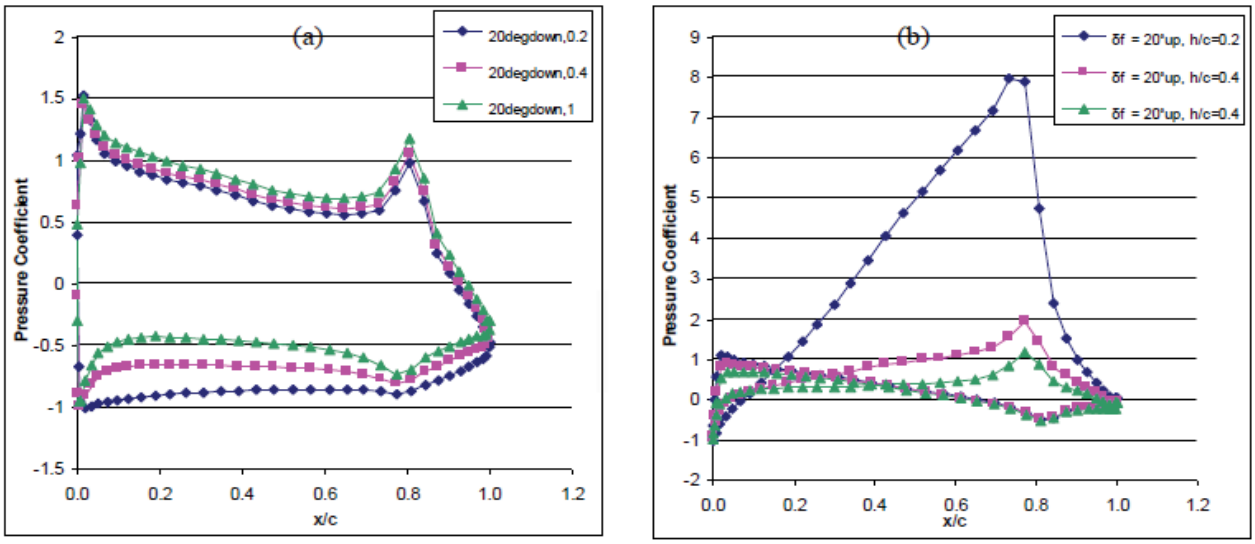

Figure 17: Pressure distribution for a NACA 2412 airfoil with aileron in ground effect, α = 3° (FEMLAB).

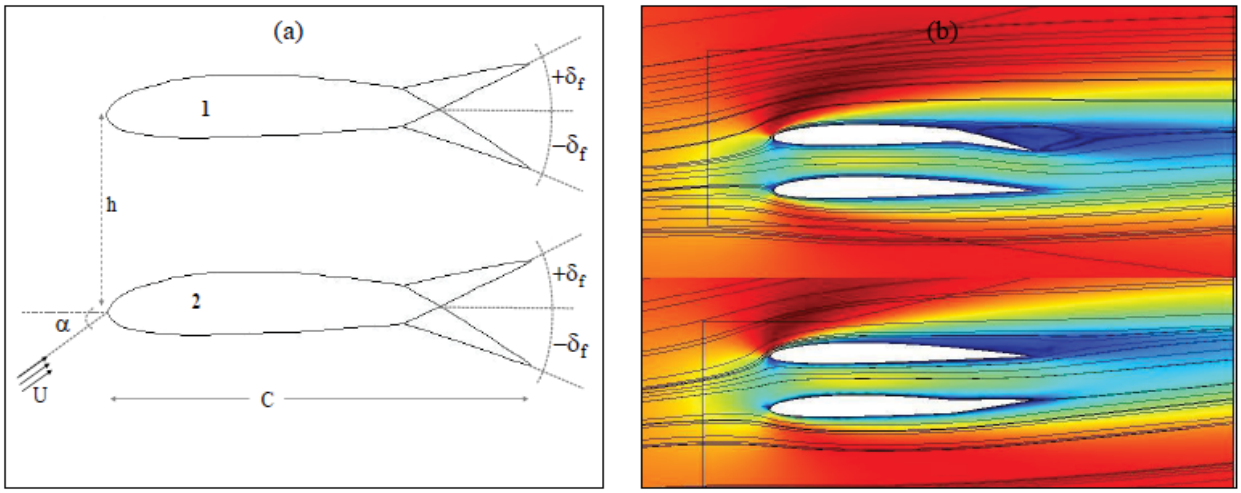

Figure 18: (a) Configuration of biplane (left) and (b) flow field velocity contours (right) for a biplane with aileron deflection.

the ground; but as it is shown in Figure 17b**,** when $\delta_f = +20°$ the pressure of the lower surface changes rapidly and reaches 8 at the aileron joint.

Ailerons in biplanes: In this section, the effect of ailerons in biplane configurations on the lift coefficient (C_L) is examined. Figure 18a and 18b show the configuration and flow field for a biplane with aileron deflection. The difference between aileron deflection in upper and lower airfoils and their effect on the lift coefficient are shown in Figure 19a and 19b. For a high aileron deflection and attack angle, C_L can reach as high as 4. Additionally, Figure 19b shows that the choice of the airfoil for aileron deflection has little or no significant effect on lift coefficient for h/c >0.5.

Conclusions

The flow field over an airfoil with 20% aileron has been numerically examined using panel and finite volume methods. Many parameters play important roles in the efficiency of the airfoil. The effects of the attack angle of the airfoil, the flap length, flap deflection angle and Reynolds number are investigated in this paper. Also, viscous flows over the flapping airfoil with different flap combinations are computed. The results of both Panel and the Volume numerical methods are consistent are in agreement with the experimental results. The results also indicate that the existence of an aileron has significant impacts on the lift and moment of the airfoil. The use of ailerons in ground effect and biplane configurations relevant to levitated high speed train has been studied as well. The following conclusions are drawn:

- For the airfoil with aileron when the attack angle is increased, the lift is also increased by two folds.
- When the aileron is upward, the pressure coefficient has a considerable change approximately at the middle of the airfoil. There are two pressure peaks at the lower and upper surfaces of the airfoil for $\delta_f \neq 0$. The deviation of these pressure peaks from the normal case ($\delta_f = 0$) is larger when the aileron is downward.

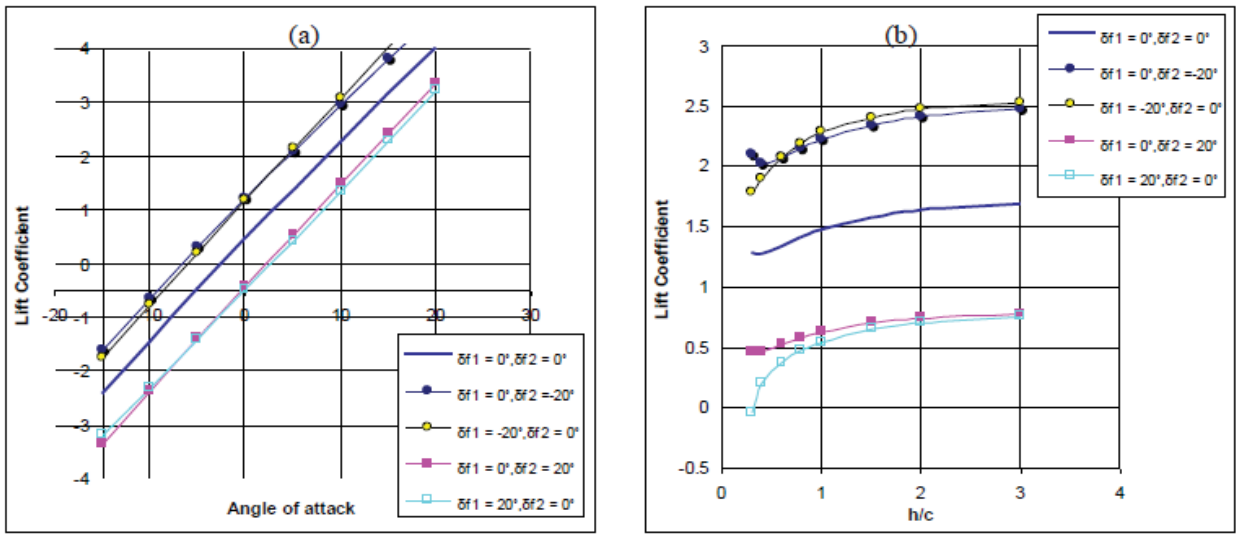

Figure 19: Lift coefficients (using FEMLAB) in biplane with aileron deflection due to: **(a)** angle of attack; **(b)** distance between the airfoils.

- When the airfoil-aileron configuration is close to the ground surface, force characteristics increase significantly and when the ride height is less than 0.15*c*, the lift coefficient decreases rapidly for $\alpha > 10°$.
- For the biplane case, the choice of the airfoil for aileron deflection has little or no important effect on lift coefficient for h/c >0.5. However, it is shown that when the deflection is on the lower airfoil, the pressure coefficient of the upper airfoil has an unexpected distribution among the surfaces of the airfoil.

References

1. Valarezo WO, Dominik CJ, Mcghee RJ, Goodman WL, Paschal KB (1991) Multi-element airfoil optimization for maximum lift at high Reynolds numbers. Technical Papers 2: 969-976.
2. Besnard E (1998) Two-dimensional aircraft high lift system design and optimization. Aerospace Sciences Meeting and Exhibit 36th Reno NV.
3. Sommerer A (2000) Numerical optimization of adaptive transonic airfoils with variable camber. International Congress of Aeronautical Sciences 22nd Harrogate United Kingdom International Organization .
4. Levy D (2007) Reynolds number effects on the performance of a hinged slotted flap. 45th AIAA Aerospace Sciences Meeting Reno NV United States.
5. Birch D (2005) Effect of trailing-edge flap on a tip vortex. J Aircraft 42 : 442-447.
6. Rinoie K (2003) Benefit and performance of various vortex flap configurations. J Aircraft 40: 1215-1218.
7. Zerihan J, Zhang Xin (2000) Aerodynamics of a Single Element Wing in Ground Effect. AIAA Journal.
8. Zhang X, Zerihan J (2003) Aerodynamics of a double-Element Wing in Ground effect. Advances in Computational Methods in Fluid Dynamics ASME New York 1994 FED41: 1007-1016.
9. Maruyama D (2006) Aerodynamic analyses of airfoil configurations of biplane type supersonic transport. J stage 72: 2132-2139.
10. Anderson, David, Eberhardt S (1988) Understanding Flight. 2nd edn. Prentice Hall.
11. US Centennial of Flight Commission. Airfoil Diagram.
12. Alexander Greg NACA Airfoil Series.
13. Pedreiro N (1999) Aileron effectiveness at high angles of attack Interaction with forebody blowing. J Aircraft 36: 981-986.
14. Li, XQ (2004) Computation of a wing-body combination with aileron.